CHARACTERIZATION OF THE PERFORMANCE OF A MINIBUBBLE GENERATOR IN CONDITIONS RELEVANT TO MICROGRAVITY

S. Arias [a], R. González-Cinca [a,b], X. Ruiz[c,d], L. Ramírez-Piscina[b,d] and J. Casademunt[d,e]
[a] Escola Politècnica Superior de Castelldefels
Universitat Politècnica de Catalunya, Esteve Terradas 5, 08860 Castelldefels (Barcelona), Spain
[b] Departament de Física Aplicada, Universitat Politècnica de Catalunya, Barcelona (Spain)
[c] Área de Física Aplicada, Universitat Rovira i Virgili Tarragona (Spain)
[d] Institut d'Estudis Espacials de Catalunya, IEEC, Barcelona (Spain)
[e] Departament d'Estructura i Constituents de la Matèria, Facultat de Física, Universitat de Barcelona, Barcelona (Spain)

ABSTRACT

We perform a characterization of a recently reported minibubbles (bubbles with a diameter of the order of 10^{-3} m) generator in microgravity related conditions. Generation of bubbles is based on the generation of a slug flow in a capillary T-junction, whose operation is robust to changes in the gravity level. We address questions regarding the performance under different working regimes. In particular, we focus on the regimes found within a large range of gas and liquid injection flow rates. The injection performance is characterized by measuring bubble generation frequency. We propose curves obtained empirically for the behavior of generation frequency and crossover between regimes.

Keywords Two-phase flow; Microgravity; Flow patterns; Bubble and slug flows; Minichannel

1. Introduction

Bubble generation and management are some of the key issues in the current research on multiphase flows for space applications [1-3]. The absence of the buoyancy force in the microgravity environment makes necessary specific methods to detach bubbles from the generator device. Typically the liquid flow is used to aid bubble detachment, both in co-flow configuration [4], in which liquid flows parallel to the gas injection direction, and cross-flow configuration [5], in which liquid flows perpendicularly to the gas injection. We proposed a configuration [6] which is a particular case of the cross-flow one. A gas and a liquid flow are injected separately into a T-junction with circular section capillaries of the same diameter (1 mm i.d.). At the T-junction, gas bubbles are formed by the action of the liquid cross-flow [6,7]. In the nominal regime of the bubble generator, capillary forces dominate over buoyancy (small Bond number[1], B_0 =0.138), and over inertial forces (small Weber number[2], *We* from $6\cdot10^{-3}$ to 22). Laminar regime can be also assumed (*Re* from 20 to 1273). Bubble formation thus results from the competition between capillary forces and the drag due to the liquid cross-flow (note that the drag can be large even in the small flow limit when the forming bubble occupies the available cross-section of the capillary). This force balance determines bubble size and generation frequency.

In this paper we report a characterization of the T-junction minibubble generation and detachment method. Larger parameter ranges than those used in [7] have been considered in this study. This has allowed for exploring different operating regimes of the bubble generator, for which a quantitative expression for the generation frequency has been obtained.

2. Experimental setup

A sketch of the experimental setup used in this work is shown in Fig. 1. It consists of the test section, data acquisition and air and water supply systems.

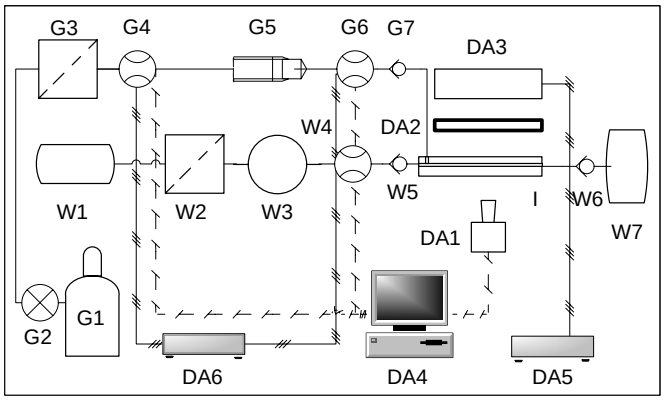

Fig. 1. Experimental setup: Test section (I: injector); Data acquisition system (DA1: high speed camera, DA2: diffuser, DA3: light source, DA4: server, DA5 and DA6: power supply); Air supply system (G1: air bottle, G2: two stages pressure reducer, G3: filter,

[1] $B_o = \frac{(\rho_l - \rho_g) g \phi_c^2}{\sigma}$, ρ_l and ρ_g being the liquid and gas densities, respectively, g the gravity, ϕ_c the capillary diameter and σ the liquid surface tension.

[2] $We = \frac{\rho_l U_{SL}^2 \phi_c}{\sigma}$, U_{SL} being the liquid superficial velocity.

G4: pressure controller, G5: chocked orifice, G6: air mass flow meter, G7: anti-return valve); Water supply system (W1: water tank, W2: filter, W3: pump, W4: water mass flow meter, W5: anti-return valve, W6: anti-return valve, W7: waste bag).

2.1. Test section

The bubble generator consists of a T-junction formed by two 1 mm diameter methacrylate capillaries (see Fig. 2) where the cross-flow between gas and liquid is promoted. Each capillary is fed by the air and water supply systems, respectively.

2.2. Data acquisition system

The bubble generator has an outer square cross-section to avoid curved surfaces, which allows recording the formation and detachment of the bubbles without optical distortions. A high speed video camera, with a CMOS sensor operating at 4000 fps, was focused at the T-junction. Rear lighting is provided by a light source with ultra bright white LEDs of 7000 mcd. A holographic diffuser sheet was used to homogenize light in order to enhance the image at the gas-liquid interface.

2.3. Air supply system

Synthetic and filtered air was used to avoid undesired particles. Air was driven through the capillary under constant mass flow rate with uncertainties in the measurement lower than 0.50 ml/min. Mass flow rate was regulated using a chocked orifice. To such end, a Bronkhorst Hi-Tec's air mass pressure controller/meter regulated the pressure of the air at the chocked orifice inlet. The air flow rate was measured before entering the T-junction by a Bronkhorst Hi-Tec's air mass flow meter (F-201C9 series). The temperature was maintained at approximately 25ºC.

2.4. Water supply system

An Ismatec MCP-Z water pump was used to manage water inside the liquid circuit. Distilled and filtered water was stored in a water tank from which water was pumped. Water flow rate was measured at the inlet of the capillary by a Bronkhorst Hi-Tec's liquid flow mass meter (L30 series) with uncertainties lower than 0.50 ml/min. Residual air and water flows coming from the bubble generator were accumulated into a residual tank.

3. Results and discussion

Experiments were performed on ground under microgravity relevant conditions at several liquid and gas volumetric flow rates, Q_L and Q_G, respectively. The cross-section averaged water and air velocities, this is, the superficial liquid and gas velocities, U_{SL} and U_{SG} , were obtained from the water and air volumetric flow rates, $U_{SL}=Q_L/A$, $U_{SG}=Q_G/A$, being A the cross-section. Values of U_{SL} ranged between 0.02 and 1.27 m/s, while U_{SG} ranged between 0.03 and 2.10 m/s. Measurement of the bubble generation frequency, f, was carried out by an image processing software. The largest frequency achieved was around 900 bubbles per second, which was correctly resolved by the image acquisition system. Frequency aliasing was avoided in each case.

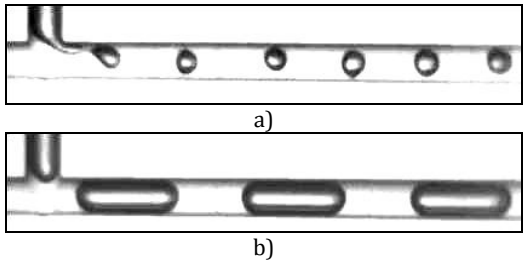

Fig. 2. Flow generation at the T-junction and flow patterns in the 1 mm i.d. minichannel: a) bubble, and b) slug.

Bubble, slug, churn and annular flows were observed, as expected in microgravity conditions [8]. Gas flows periodically distributed in bubble and slug regimes. Whereas gas forms discrete bubbles inside the liquid phase in bubble flow (Fig. 2-a), bullet-shaped bubbles occupy almost the entire minichannel cross-section in slug flow (Fig. 2-b). Under laminar conditions, the bubble generator is characterized by small bubble size dispersion and high regularity in bubble generation for both bubble and slug regimes [7].

Dependence of the bubble frequency with the superficial gas velocity at different superficial liquid velocity is shown in Fig. 3. Data analysed here cover a much broader region of U_{SL} and U_{SG} values than in [7]. Points correspond to slug (mainly) and bubble flow regimes, although churn and annular regimes have also been observed at low U_{SL} and high U_{SG}. This parameter region corresponds to the lower right corner of the figure and explains why no frequency was measured there due to the lost of bubble generation regularity in churn and annular regimes.

The behavior of the bubble frequency shows two distinguishable regimes, as it was already found in [7]: a linear regime at low U_{SG}, and a saturation regime at larger U_{SG} values. The linear behaviour is a consequence of the bubble size being independent from the gas flow rate for small fluxes [6]. The physical idea is that in this regime the detachment of the forming bubble at the T-junction occurs when the drag with the liquid is large enough to overcome capillary forces [6]. On the contrary, for large gas flow rates there is a limiting scale for the bubble generation process, which is the time needed by the liquid flow to cross a distance of the order of the capillary diameter [7]. This produces a maximum value of the generation frequency for each value of the liquid flow rate. This is the origin of the saturation regime.

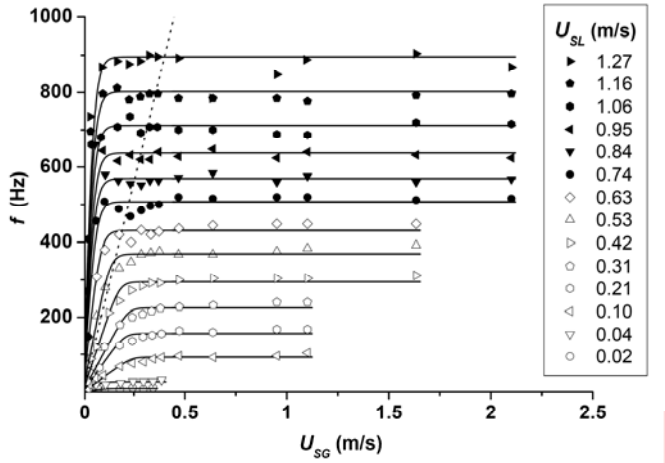

Fig. 3. Bubble frequency as a function of the superficial gas velocity U_{SG} for different superficial liquid velocities U_{SL}. *Symbols:* experimental results, *lines:* fit (Eq. (1)), *dot line:* separation between bubble (left) and slug (right) flow regimes.

Lines in Fig. 3 correspond to data fitting by standard nonlinear regressions to

$$f(U_{SG},U_{SL}) = f_{sat} - a\cdot\varepsilon\cdot\log\left(1+\exp\left(\frac{U_{SG0}-U_{SG}}{\varepsilon}\right)\right), \qquad (1)$$

Eq. (1) is defined as a simple function with a qualitative behaviour interpolating between a linear function and a constant saturation value. Such behavior involves three parameters: the slope of the initial region, a, the scale of the crossover region, ε, and the value of the final constant value, $f_{sat}=a\cdot U_{SG0}$. Then U_{SG0} is the superficial gas velocity at the crossover point between linear and saturation regimes, defined as the point where a line starting at the origin with a slope a intersects the horizontal line of the saturation region. Of these three parameters two of them carry a clear physical meaning and can be related to theoretical considerations, namely the initial slope (related to the bubble size, which in this regime is expected to depend only on the liquid flow [6]) and the saturation frequency (also related with the liquid flow [7]). The length of the crossover region is of no clear interest as long as it is small enough for allowing both regimes to be observable and does have a negligible effect on the computed results for the other two, physically more relevant, parameters. For the sake of clarity and due to the fact that ε did not give any new physical insight it has been chosen as the superficial velocity corresponding to the characteristic volumetric flow rate of $Q*=1$ml/min, thus being $\varepsilon = Q*/A=1/(15\pi)$ m/s. Results on fitted values of a and f_{sat} did not depend on the precise value chosen for ε. This fitting curve is designed to match theory [6,7] in the following aspects:

i) at $U_{SG} << U_{SG0}$, $f(U_{SG})=a\cdot U_{SG}$, which coincides with the linear behavior predicted theoretically.

ii) the averaged bubble diameter, ϕ_B, does not vary at low U_{SG}. It can be estimated from the bubble generation frequency and the average volume of a bubble V_B:

$$Q_G = f\cdot V_B = f\cdot\left(\frac{\pi}{6}\phi_B^{\,3}\right), \qquad (2)$$

which leads to

$$\phi_B = \sqrt[3]{\frac{6}{\pi}\frac{Q_G}{f}} = \sqrt[3]{\frac{6A}{\pi}\frac{U_{SG}}{f}} \xrightarrow{U_{SG}\to 0} \sqrt[3]{\frac{6A}{\pi}\frac{1}{a}}, \qquad (3)$$

Thus, Eq. (1) gives a prediction for the bubble generation frequency at given values of U_{SL} and U_{SG} which is consistent with the existing theory for the linear regime.

The averaged bubble diameter normalized with the capillary diameter ϕ as a function of the superficial gas velocity is plotted in Fig. 4. Bubble and slug regimes can be then distinguished by the value $\phi_B/\phi=1$ in this figure, according with Dukler criterion [8].

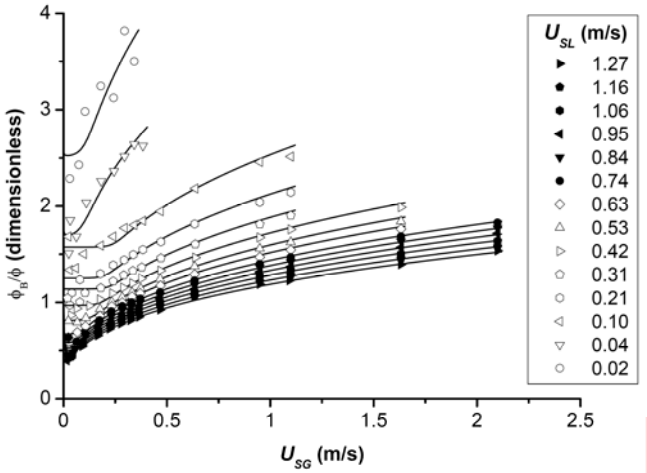

Fig. 4. Dependence of the averaged dimensionless bubble diameter, ϕ_B/ϕ, with the superficial gas velocity, U_{SG}. *Symbols:* experimental data, *lines:* fit (Eq. (3)).

The saturation frequency was computed for every superficial liquid velocity considered, showing a linear behavior. The experimental values are shown in Fig. 5 together with the fitting line (expressed in the figure units):

$$f_{sat}(U_{SL}) = 719.6\cdot U_{SL} - 14.4 \qquad (4)$$

Dot line in Fig. 5 corresponds to the theoretical prediction in [7]. The fitting line has a very similar slope than the one obtained in [7], in which fewer points were considered.

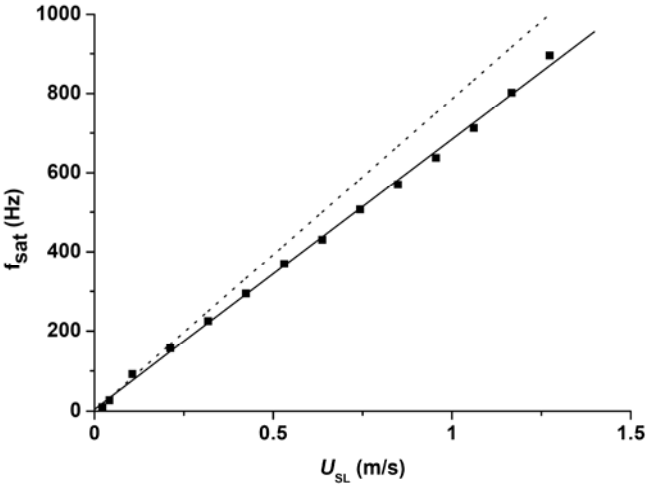

Fig. 5. Saturation frequency as a function of the superficial liquid velocity. *Symbols:* experimental data, *line:* linear fit (Eq. (4)), *dot line:* theoretical prediction.

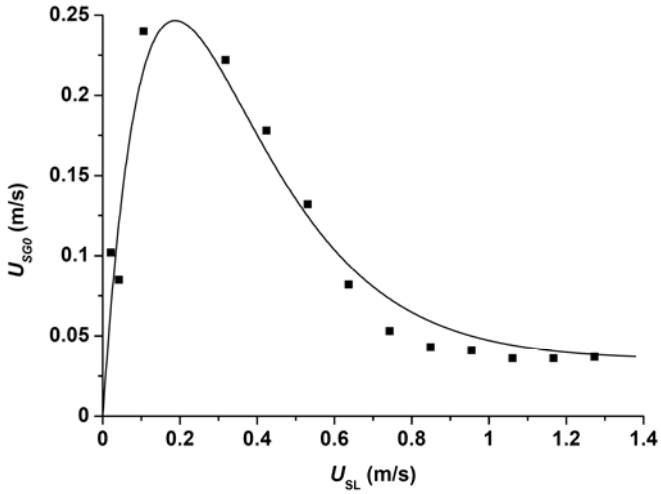

Fig. 6. Crossover point as a function of the superficial liquid velocity. *Symbols:* experimental data, *line:* fit (Eq. (5)).

The crossover point was computed after its definition for every superficial liquid velocity considered (see Fig. 6). Points were fitted taking into account the following features:

i) at large values of U_{SL}, U_{SG0} tends to a finite value different to zero.
ii) at very low values of U_{SL}, f_{sat} tends to zero and a to a constant value. Thus U_{SG0} tends to zero too.

The proposed fitting curve for the variation of the crossover point with U_{SL}, expressed in the figure units, is:

$$U_{SG0}(U_{SL}) = 3.25\left(0.01 + (U_{SL} - 0.01)\exp\left(-\frac{U_{SL} - 0.01}{0.18}\right)\right) \quad (5)$$

This fitting curve tends to a horizontal asymptote U_{SGO}=0.0325 m/s at large values of U_{SL}.

The initial slope of the linear regime obtained from experimental data in Fig. 3 is shown in Fig. 7. Combining Eqs. 4 and 5 with

$$a(U_{SL}) = \frac{f_{sat}(U_{SL})}{U_{SG0}(U_{SL})} \quad (6)$$

one obtains the fitting curve shown in Fig. 7. Both experimental points and fit show an exponential behavior at low superficial liquid velocities which turns to a linear tendency for higher U_{SL}. This linear asymptotic tendency, which is also shown in the figure, can be expressed by (in the figure units)

$$a_{asint}(U_{SL}) = 22141.5 \cdot U_{SL} - 444.4 \quad (7)$$

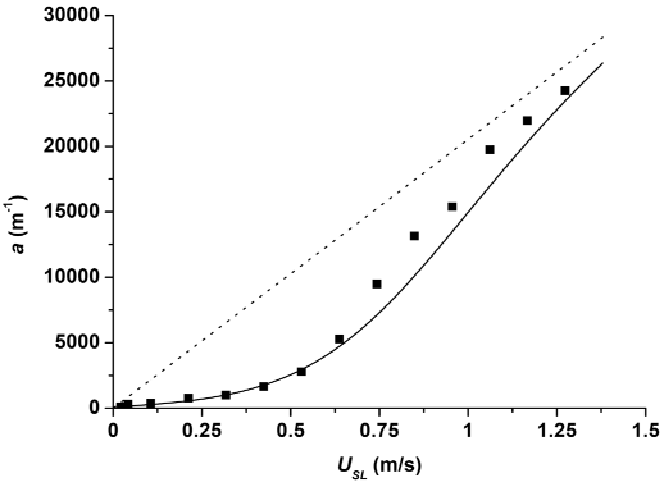

Fig. 7. Initial slope of the linear regimen as a function of the superficial liquid velocity. *Symbols:* experimental data, *line:* fit (Eq. (6)), *dot line:* linear asymptotic tendency (Eq. (7)).

4. Conclusions

We have presented an experimental characterization of a minibubble generator for a broad range of gas and liquid flow rates. The key of the bubble generation method is that performance in normal gravity and microgravity conditions does not show significant differences due to the small value of the Bond number. Additional advantages are reachable high bubble generation frequencies, controllable bubble diameter of the order of the capillary and reduced bubble size dispersion. Bubble, slug, churn and annular flow regimes have been observed.

Bubble frequency at different superficial gas velocities presents a linear behavior followed by a saturation state, showing a good agreement with existing theoretical predictions [6,7]. A new expression for the bubble generation frequency at given values of U_{SL} and U_{SG} has been proposed. Results obtained confirm the linear

behavior of the saturation frequency with the superficial liquid velocity. A new expression has been proposed for the crossover point between linear and saturation regimes at different superficial liquid velocities. The variation of the crossover point and the slope of the linear regime with the superficial liquid velocity have both been found to present a linear asymptotic tendency.

Acknowledgements

We acknowledge financial support by Ministerio de Educación y Ciencia (Projects number FIS2006-11452-C03-02, FIS2006-03525 and ESP2007-30637-E, Spain).

References

[1] J. McQuillen, C. Colin and J. Fabre, Ground-based gas-liquid flow research in microgravity conditions: state of knowledge, Space Forum 3, 165-203 (1998).
[2] H. Ohta, A. Baba, K. Gabriel, Review of existing research on microgravity boiling and two-phase flow, Ann. N.Y. Acad. Sci. 974, 410-417 (2002).
[3] A. A. Kulkarni, J.B. Joshi, Bubble formation and bubble rise in gas-liquid system: a review, Ind. Eng. Chem. Res. 44, 5873-5931 (2005).
[4] A. Bhunia, S.C. Pais, Y. Kamotani and I. Kim, Bubble formation in a coflow configurations in normal and reduced gravity, AIChE J. 44, 1499-1509 (1998).
[5] S.E. Forrester, C.D. Rielly, Bubble formation from cylindrical, flat and concave sections exposed to a strong liquid cross-flow, Chem. Eng. Sci. 53, 1517-1527 (1998).
[6] J. Carrera, X. Ruiz, L. Ramírez-Piscina, J. Casademunt, M. Dreyer, Generation of a monodisperse microbubble jet in microgravity, AIAA J 46, 2010-2019 (2008).
[7] S. Arias, X. Ruiz, L. Ramírez-Piscina, J. Casademunt, R. González-Cinca, Experimental study of a microchannel bubble injector for microgravity applications, Microgravity Sci. and Technol 21 107-111 (2009).
[8] A.E. Dukler, J. A. Fabre, J. B. McQuillen, R. Vernon, Gas-liquid flow at microgravity conditions: flow patterns and their transitions, International Journal of Multiphase Flow 14, 389–400 (1988).